A low-friction graphene nanoplatelets film from suspension high velocity oxy-fuel thermal spray

Cite as: AIP Advances **9**, 025216 (2019); https://doi.org/10.1063/1.5089021
Submitted: 16 January 2019 . Accepted: 13 February 2019 . Published Online: 21 February 2019

F. Venturi, G. A. Rance, J. Thomas, and T. Hussain

A low-friction graphene nanoplatelets film from suspension high velocity oxy-fuel thermal spray

Cite as: AIP Advances 9, 025216 (2019); doi: 10.1063/1.5089021
Submitted: 16 January 2019 • Accepted: 13 February 2019 •
Published Online: 21 February 2019

F. Venturi,[1] G. A. Rance,[2] J. Thomas,[3] and T. Hussain[1,a)]

AFFILIATIONS

[1]Faculty of Engineering, University of Nottingham, Nottingham NG7 2RD, UK
[2]Nanoscale and Microscale Research Centre, University of Nottingham, Nottingham NG7 2RD, UK
[3]School of Physics and Astronomy, University of Nottingham, Nottingham NG7 2RD, UK

[a)]**Corresponding author. E-mail:** tanvir.hussain@nottingham.ac.uk

ABSTRACT

The addition of graphene-based nanomaterials is known to improve the tribology properties of materials by lowering the coefficient of friction and reducing wear. The covering of small areas with thin graphene-based films is routinely carried out; however, a fast and efficient way of covering large areas represents an outstanding challenge. Here we present a method for the deposition of graphene nanoplatelets (GNPs) on stainless steel substrates based on suspension high-velocity oxy fuel thermal spray. GNPs were radially injected into the combustion jet, providing sufficient momentum and moderate heat transfer to facilitate effective bonding with the substrate. Upon unlubricated ball-on-disc wear testing against an alumina counterbody, GNPs undergo gradual exfoliation, covering the substrate and thus lowering the friction coefficient (<0.1). We have reported the formation of a thin layer, composed of GNPs having different amounts of disorder, which protects the underlying substrate from wear. GNP structural ordering is studied throughout deposition and wear tests, showing an increase of inter- and intralayer disorder at the nanoscale, whilst largely preserving the GNP microstructure.

The durability of moving mechanical parts, as well as their ability to withstand repeat movements under load without significant damage or heating, is a longstanding issue far from being fully solved. It has been calculated[1] that 23% of the world's energy usage finds its origin in friction or the fabrication of parts which need replacement due to wear, with a major impact on both the economy and the environment. Tackling this issue would require low friction and wear resistant materials and coatings. Alongside its remarkable and well-known mechanical,[2] thermal,[3] electrical[4] and optical[5] properties, the tribological performance of graphene has attracted wide interest in recent years.[6] At the nanoscale, graphene exhibits low frictional force[7] which can be further improved by using multi-layered graphene, thus exploiting the lubricating characteristics of lamellar solids,[8] or by providing an optimal graphene-substrate binding to hinder the puckering effect[9] i.e. out-of-plane elastic deformation which is a major cause for single layer graphene friction. Also, the wear resistance of graphene itself has been shown to improve when using few-layer graphene.[10] The ordinary, well-established methods for graphene deposition are either cheap and fast but with uncontrolled outcome, like scotch-tape exfoliation,[11] or accurate at the atomic level but slow and non-scalable, like chemical vapor deposition.[12] Graphene nanoplatelets (GNPs), which are normally composed of 15-20 graphene layers, are good candidates for obtaining lubricating films that can reduce friction and protect the underlying substrate from mechanical wear. According to thermogravimetric measurements,[13,14] GNPs are more stable than graphene at temperatures up to 700°C due to their lower surface to volume ratio. GNPs provide the advantage of interlayer shear to reduce friction but also keep graphene-like mechanical properties, are more resistant and easier to handle than single layer graphene and they can be deposited using a wide variety of methods. Spray depositions for instance are a scalable method, which can provide fast and versatile coverage of graphene-based

materials on extended surfaces.[15] Among these, airbrush spray[16] and supersonic cold spray[17] lead to good coverage, but due to low kinetic energy or low temperature they do not favor an optimal adhesion to the substrate, for which the addition of polymers would be needed.[18,19] Thermal spray, on the other hand, can provide sufficient particle velocity and temperature to a wide range of particle sizes that can adhere to a surface rapidly. Suspension High-Velocity Oxy Fuel (S-HVOF) thermal spray locates in this framework as a promising means for the deposition of GNPs, mainly due to the reliability, scalability and cost-effectiveness of the process.[20] SHVOF thermal spray allows a liquid carrier to be utilized for GNPs, which can minimize particle handling risks, and the process enables particles to be accelerated by a supersonic combustion flame in a very short time. Moreover, conversely to cold spray techniques, the high temperature flame heats the substrate, enhancing the coating adhesion onto it. Feedstock injection into the flame is a critical point in SHVOF, as at this stage GNPs degradation can occur. Axial injection was proved suitable for GNP/Alumina nanocomposites,[21] but in case of GNP-only feedstock it can lead to structural changes in the GNPs at the nanoscale. Conversely, radial injection can deliver to the feedstock a smaller, tunable amount of heat as the injection position and direction can have a noticeable effect on heat transfer, atomization, agglomeration and melting of the injected particles. Radial injection is the ordinary setup for other thermal spray techniques as plasma spray, but has been rarely employed in HVOF thermal spray and is here presented for the first time for depositing graphene-based materials.

The setup we propose here is based on a commercial Top-Gun SS (GTV GmbH, Germany) suspension spray gun, where the feedstock is injected radially using a 450 μm diameter injector pointed towards the jet with 15° downstream tilt at 10 mm from the gun exit. The choice of this combination of parameters follows an optimization process that aimed at maximizing feedstock penetration in the jet and momentum transfer, while minimizing its permanence in the jet to hinder mechanical and thermal degradation of GNPs. The experimental setup and injection imaging are shown in supplementary material Figure S1. The feedstock suspension is water-based and contains 1 wt.% GNPs (nominally 5 μm wide, 5-8 nm thick). The SHVOF gun is operated using 151 l/min oxygen flow rate and 354 l/min hydrogen flow rate. The GNPs were sprayed on 304 stainless steel (SS) substrates mounted at 300 mm stand-off distance on a rotating carousel, for a total spray time of 4 minutes with a feedstock flowrate of 170 ml/min. The stand-off distance is high if compared to the ordinary ones used in SHVOF (~100 mm). This prevents the substrate from overheating, reducing the damaging of GNPs already deposited on it. Measurements carried out with an infrared thermometer right after spray showed a temperature of 80 °C, significantly lower than that required to initiate thermal degradation of GNPs.[13]

The sample top surface morphology analyzed by Scanning Electron Microscopy (SEM) (JEOL, Japan) is shown in Figure 1a. This image shows an overview of the GNPs-covered SS surface, exhibiting an even coverage of GNPs with varying thickness. As explained in Ref. 22, graphene hinders the signal of the secondary electrons generated by the substrate, making thicker areas appear darker. The very bright spots are instead particles charging under the beam as they are only partially adherent to the underlying GNPs or substrate. It is also possible to distinguish some light grey areas where the GNPs layer thickness is none or minimal. Measurements carried out throughout the sample, over a total area of 3.5 mm^2, showed that these areas are (8 ± 1) % of the whole surface. Higher resolution images obtained with Field Emission Gun (FEG) SEM shown in Figure 1b allow better insight into the microstructure of an area of densely packed GNPs, revealing a stratification of GNPs stacked in a parallel fashion on top of each other. In conventional thermal spray, particles melt in-flight and solidify at the substrate, providing good bonding and coating build-up. Here, due to radial injection, GNPs are not heated to melting point, but are still accelerated sufficiently; the bonding mechanism is therefore more akin to the cold spray.[23] Also, some of the GNPs which are not accelerated sufficiently lie loosely on the top surface due to a weaker bonding mainly due to van der Waals attraction.

However, the amount of thermal and mechanical shock GNPs undergo when sprayed is high as revealed by the presence of GNPs in the sample which are far smaller (~100 nm) than the nominal size (5 μm). It is therefore important to assess the structural integrity of GNPs as they are processed into suspension or sprayed. The structural analysis on GNPs at the different stages of the process was carried out using Raman spectroscopy on a LabRAM Raman microscope (Horiba, UK). For each sample, 400 spectra were acquired over 40x40 μm areas; this statistical analysis approach was employed to allow meaningful comparison of the relative intensities of the peaks

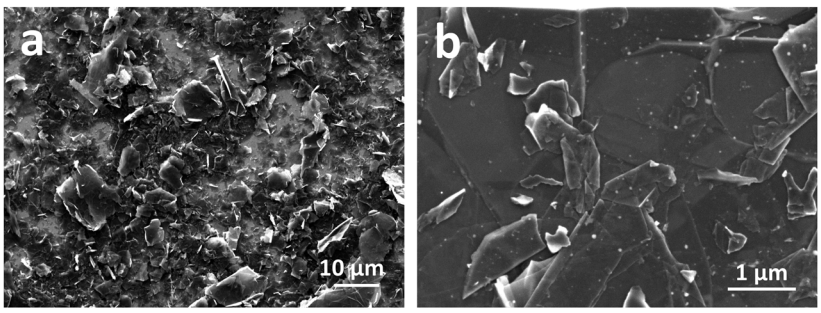

FIG. 1. SEM images of sprayed GNPs – (a) Plane view SEM image of the sample at low magnification, showing a well-dispersed coverage with dense and sparse areas, with some of the bigger GNPs randomly oriented with respect to the substrate plane. (b) High resolution FEG SEM image of a densely packed area, showing the parallel stacking of GNPs on top of each other.

TABLE I. Intensity ratios of the D and 2D bands with respect to the G band (I_D:I_G and I_{2D}:I_G) indicating the amount of intra- and interlayer disorder, respectively. The uncertainty associated to the measurements is the standard deviation of the mean.

	I_D:I_G (intralayer disorder)	L_D (nm) (distance between defects)	I_{2D}:I_G (interlayer disorder)
GNP powder	0.19 ± 0.10	27.7	0.25 ± 0.04
GNP suspension	0.24 ± 0.13	24.7	0.24 ± 0.08
GNP sprayed	0.25 ± 0.12	24.1	0.23 ± 0.05

present in the spectra in order to yield information on the presence and type of defects in GNPs. A typical Raman spectral profile of GNPs comprises three principle peaks, namely the D, G and 2D bands, observed at around 1350, 1582 and 2700 cm^{-1}, respectively, using 515 nm laser excitation.[24] The G (graphite) band is the main in-plane vibrational mode of the graphitic lattice, present in all graphitic nanostructures and therefore is typically used as internal reference. The D (disorder) band is a ring-breathing vibrational mode that arises due to the presence of point defects, such as vacancies or substitutional atoms. Therefore, the intensity ratio of D and G bands can be used to diagnose intralayer ordering, with a higher I_D:I_G a clear indicator of disorder within the graphene layers in the GNPs. The extent of this ordering can be quantified as a distance between defects, $L_D = 1.8x10^{-9}(\lambda^4(I_D:I_G)^{-1})^{1/2}$.[25] The intensity, shape and position of the 2D band – the second order of the D band – are diagnostic of interlayer ordering: intense, narrow in width and red-shifted in position for ordered nanocarbons, such as few-layer graphene and highly oriented pyrolytic graphite; dampened, broadened and blue-shifted for more disordered structures, including turbostratic graphite and amorphous carbons.[26] We will refer to the defects manifested by changes in the I_D:I_G and I_{2D}:I_G bands ratios as intralayer and interlayer disorder, respectively.

The statistical Raman spectroscopy analysis highlighted a slight increase in intralayer disorder (I_D:I_G increases) upon suspension of GNPs in water – a process which involves ultrasonication – with no further changes induced during spraying. Moreover, no significant difference in intralayer ordering (I_{2D}:I_G remains reasonably constant) during both stages of processing was observed, as reported in Table I. In addition, the distribution of GNPs on the SS substrate appears to be uniform (Figure S2). No measurable structural changes were identified from X-ray diffraction analysis (Figure S3).

The tribology performance of the deposited GNP films was studied using a ball-on-disc tribometer (Ducom instruments, The Netherlands) with a 6 mm diameter Al_2O_3 counterbody. Wear tests were carried out at 2, 5 and 10 N load, along circular paths of 10 mm diameter at an angular velocity of 60 RPM for 2000 cycles. A reference SS-only wear test was carried out at 2 N load only. The sinusoidal signal due to sample levelling imperfection has been removed using Fourier transform methods.[27] The wear tests are characterized by a low friction regime (friction coefficient lower than 0.1) within the first ~1000 cycles, followed by an increase towards SS-only values, as shown in Figure 2a. The GNPs are known to form a protective layer upon wear testing[28] and to decrease the friction coefficient as a consequence of grain refinement and laminated sheets slippage.[29] The initial 250 cycles of the wear test are shown in Figure 2b. The initial spikes are caused by the counterbody building up, arranging and settling the GNPs from the initial disordered arrangement. In fact, this settling process is faster at higher loads. These spikes are then followed by a smoothly decreasing trend, where the wear-formed GNP protective layer provides the best lubricating performance. It was noted that higher loads also lead to lower values of friction coefficient, with the lowest values of 0.055 reached in the low friction regime at 10 N load. This trend has been reported[30] and attributed to the more effective formation at higher loads of a graphene protective layer. The behavior in the last ~1000 cycles in Figure 2a is then very different for the various loads. The friction coefficient generally increases at all loads, but at 2 and 5 N it is kept below 0.3, whereas at 10 N it reaches SS-only values. Also, the widths of

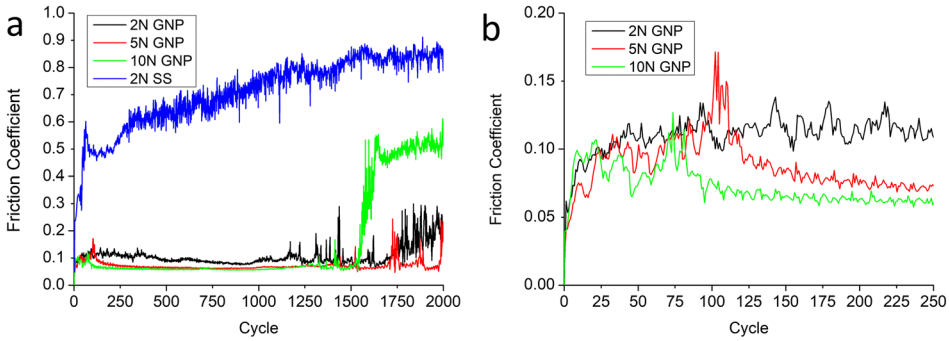

FIG. 2. Wear test results – (a) Friction coefficient of sample with GNP measured at 2, 5 and 10 N load over 2000 cycles, showing low friction coefficient regime (friction coefficient <0.1) up to 1500 cycles. A reference wear test on polished SS with no GNPs is shown for comparison, indicating a friction coefficient enhancement factor of up to 15. (b) The first 250 cycles of the wear test in (a) show friction coefficient behavior at the initial stage of the wear test, when the GNP settling takes place.

the wear tracks (not shown here) are quite different between the different loads, from (176±1) and (218±2) μm at 2 and 5 N, respectively, to (730±11) μm at 10 N load. In fact, the GNP protective layer is partially removed at 2 and 5 N, and totally removed in the 10 N case.

A deeper insight on the GNP protective layer characteristics is provided by a 2 N wear test which was stopped after 1000 cycles, when the friction coefficient is still below 0.1 and the GNP layer is almost intact. The GNP protective layer is shown in Figure 3a, and can be identified as the central dark grey area. It is worth noticing that the SEM image in Figure 1a showed a substrate not fully covered by GNPs. However, since every GNP consists of a stack of 15-20 graphene layers, upon gliding these can increase the area coverage by one order of magnitude, leading to a full, even coverage of the substrate along the contact area. The result of this process is a densely packed GNP film, where the boundaries between the different initial GNPs are no longer identifiable. On the right side of the GNP layer, some cracking is visible, as initial signs of its disruption, whereas on the left side most of it has been removed, leaving only scattered GNPs. The carbon EDX map in Figure 3b confirms carbon as the constituent element of the layer. On the right hand side of Figure 3b, some ploughing grooves are visible superimposed on substrate polishing lines, meaning that the substrate top morphology has been preserved.

The fine microstructure of the GNP layer is revealed by the AFM map in Figure 3c taken at the center of the layer. Here, the presence of small GNPs less than 1 μm wide, dispersed in a matrix of highly disordered GNPs and amorphous carbon emerges, demonstrating the range of GNP microstructures. The polishing lines can be detected through this thin soft layer.[31] The amount of structural disordering can be assessed with Raman spectroscopy, as shown in the line scan of Figure 3d, where the I_D:I_G and I_{2D}:I_G values are shown as a function of position across the wear track. It is noticeable how the values at the borders are comparable to those in Table I (I_D:I_G = 0.28±0.16, I_{2D}:I_G = 0.24±0.05) and, progressing towards the wear track center, the I_D:I_G increases (1.24±0.24), whilst I_{2D}:I_G decreases (0.09±0.06). I_D:I_G is higher at the very center of the wear track (up to a maximum of 1.67), where the contact pressure is highest, and at its borders where the GNP packing is lower and then puckering and GNP layer removal occur the most, as also shown by cracking in Figure 3a. The lower GNP packing at lower loads is also suggested by the lower minimum friction coefficient values reached at higher loads as in Figure 2a. Conversely, the lower I_{2D}:I_G values are more even across the wear track, suggesting that a threshold level has been reached, with very low interlayer coordination i.e. few layers, high disorder as in nanocrystalline graphite and amorphization (Figure S4). Most noticeably, the Raman spectrum characteristic of GNPs is preserved throughout the wear

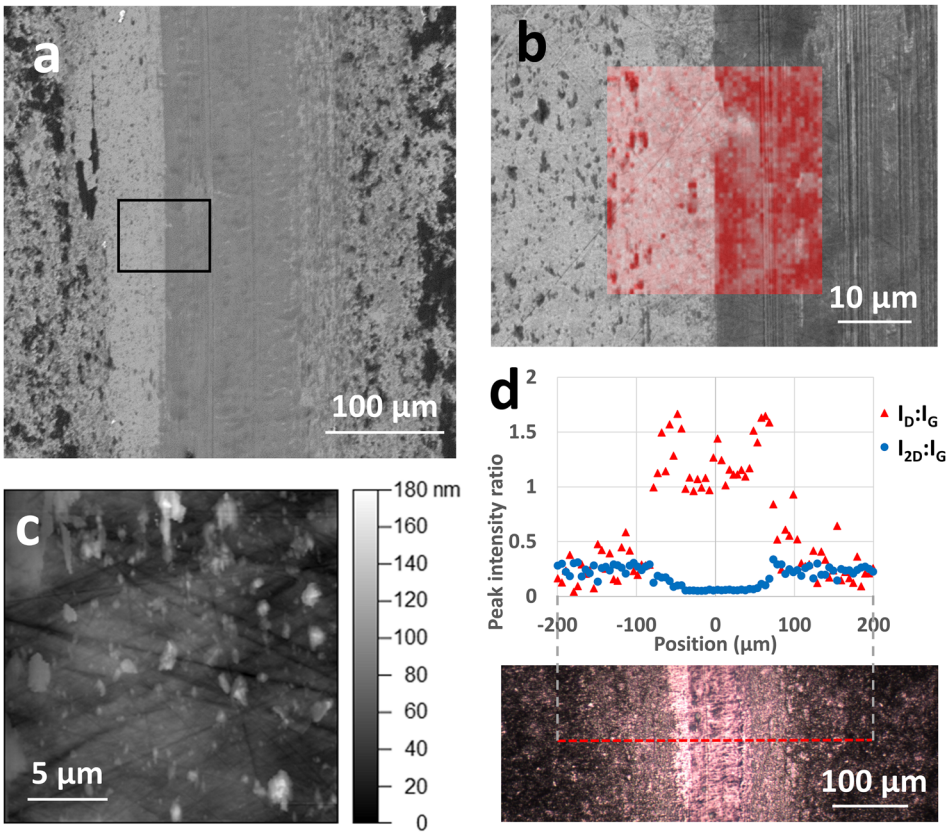

FIG. 3. Wear track characterization – (a) SEM image of 2 N load wear track after 1000 cycles. The wear-formed GNP protective layer (dark grey part) shows severe removal on the left and cracking on the right. (b) SEM image of the area marked in (a) with superimposed EDX carbon map (high intensity red coloration commensurate with high carbon content) showing the boundary between removed and non-removed GNP layer. (c) AFM height map taken at the center of the GNP layer showing its mixed nature, as it is composed of preserved and amorphized GNPs. (d) Graph displaying I_D:I_G and I_{2D}:I_G as a function of position traversing the wear track as shown in the optical microscope image below. An increase of I_D:I_G and a decrease of I_{2D}:I_G is evident at the center of the wear track, indicating GNP inter- and intralayer disordering.

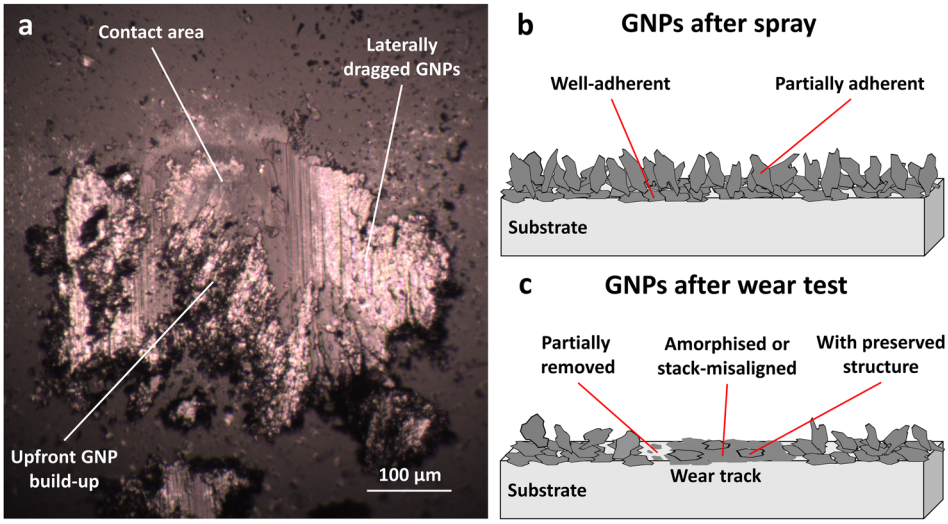

FIG. 4. Schematics of GNP removal – (a) Optical microscopy image of the counterbody after 1000 cycles at 2 N, showing a small contact area and a large amount of GNP which are adherent to the sides and to the front of the contact area either compacted or in debris form. These laterally dragged GNPs extend much further than the counterbody contact area, contributing to the removal of the GNP film outside the wear track center where the GNP protective layer is formed. (b) Sketch of sprayed GNPs layer exhibiting different degrees of adhesion. (c) Sketch of the GNP layer after the wear test, showing the protective GNP layer formation at the track center, corresponding to the counterbody contact area, and partial GNP film removal at the sides by dragged GNPs.

track, confirming the conservation of the GNP layer after 1000 wear cycles. The friction coefficient is still efficiently lowered, meaning the GNP tribological features are conserved.

A better understanding of the wear mechanism involved is given by the image of the counterbody in Figure 4a. The starting condition is presented in the schematics of Figure 4b, with a mixture of well and partially adherent GNPs. Upon wear testing, different mechanisms lead to the final condition of Figure 4c, with the presence of a partially removed GNP layer. The layer formation and structural reorganization of GNPs is due to the contact area in the very central part of the counterbody ball. Alongside, GNP stacks are built upfront and sideways and dragged along the wear track, mechanically removing GNPs at the sides of the GNP layer, which is then partially removed. Also, the effects of the dragged GNPs stack extend on a 400 um wide area, shredding and degrading GNPs.

In conclusion, SHVOF proves a suitable technique for depositing GNP films. SEM and Raman spectroscopy show >90% coverage and minor GNP structural disorder. Upon wear testing, a protective layer composed of GNPs with different degrees of structural integrity and amorphization is formed. The GNP layer lowers the friction coefficient up to a factor 15 with respect to the SS-only case, effectively protecting the underlying surface from wear. The layer is gradually removed by ploughing by the counterbody and direct mechanic removal by the GNPs dragged by it.

Additional information regarding the experimental setup, suspension preparation and injection, spray parameters, samples characterization and data analysis can be found in the supplementary material. Moreover, supplementary material figures are presented, showing the spray setup, along with high-speed injection imaging, Raman maps of the sprayed GNPs, X-rays diffractograms of pristine powder, GNP suspension and sprayed GNPs, and a comparison of the mean Raman spectra of the GNPs powder and of the sprayed GNPs both inside and outside the wear track.

This work was supported by Engineering and Physical Sciences Research Council, Impact Acceleration Account scheme [grant number EP/R511730/1]. The authors gratefully acknowledge the Nanoscale and Microscale Research Centre (nmRC) at the University of Nottingham for access to the SEM and Raman spectroscopy facilities, S. Bano for her help in XRD measurement of GNP powder and the patient and careful work of R. Screaton and J. Kirk in managing SHVOF spray.

REFERENCES

[1] K. Holmberg and A. Erdemir, Friction **5**, 263 (2017).
[2] C. Lee, X. Wei, J. W. Kysar, and J. Hone, Science **321**, 385 (2008).
[3] A. A. Balandin, Nat. Mater. **10**, 569 (2011).
[4] A. S. Mayorov, R. V. Gorbachev, S. V. Morozov, L. Britnell, R. Jalil, L. A. Ponomarenko, P. Blake, K. S. Novoselov, K. Watanabe, T. Taniguchi, and A. K. Geim, Nano Lett. **11**, 2396 (2011).
[5] F. Bonaccorso, Z. Sun, T. Hasan, and A. C. Ferrari, Nat. Photonics **4**, 611 (2010).
[6] D. Berman, A. Erdemir, and A. V. Sumant, Mater. Today **17**, 31 (2014).
[7] L.-Y. Lin, D.-E. Kim, W.-K. Kim, and S.-C. Jun, Surf. Coat. Tech. **205**, 4864 (2011).
[8] R. F. Deacon and J. F. Goodman, Proc. R. Soc. Lond. A **243**, 464 (1958).
[9] X. Zeng, Y. Peng, and H. Lang, Carbon **118**, 233 (2017).
[10] D. Berman, S. A. Deshmukh, S. K. R. S. Sankaranarayanan, A. Erdemir, and A. V. Sumant, Adv. Funct. Mater. **24**, 6640 (2014).
[11] K. S. Novoselov, A. K. Geim, S. V. Morozov, D. Jiang, Y. Zhang, S. V. Dubonos, I. V. Grigorieva, and A. A. Firsov, Science **306**, 666 (2004).
[12] X. Li, W. Cai, J. An, S. Kim, J. Nah, D. Yang, R. Piner, A. Velamakanni, I. Jung, E. Tutuc, S. K. Banerjee, L. Colombo, and R. S. Ruoff, Science **324**, 1312 (2009).
[13] L. Yu, J. S. Park, Y.-S. Lim, C. S. Lee, K. Shin, H. J. Moon, C.-M. Yang, Y. S. Lee, and J. H. Han, Nanotechnology **24**, 155604 (2013).
[14] P. Song, Z. Cao, Y. Cai, L. Zhao, Z. Fang, and S. Fu, Polymer **52**, 4001 (2011).
[15] M. J. Nine, M. A. Cole, D. N. H. Tran, and D. Losic, J. Mater. Chem. A **3**, 12580 (2015).
[16] L. David, A. Feldman, E. Mansfield, J. Lehman, and G. Singh, Sci. Rep. **4**, 4311 (2014).
[17] D.-Y. Kim, S. Sinha-Ray, J.-J. Park, J.-G. Lee, Y.-H. Cha, S.-H. Bae, J.-H. Ahn, Y. C. Jung, S. M. Kim, A. L. Yarin, and S. S. Yoon, Adv. Funct. Mater. **24**, 4986 (2014).

[18]Y. Zhang, D. Zhang, X. Wei, S. Zhong, and J. Wang, Coatings **8**, 91 (2018).
[19]T. Huang, T. Li, Y. Xin, B. Jin, Z. Chen, C. Su, H. Chen, and S. Nutt, RSC Adv. **4**, 19814 (2014).
[20]F.-L. Toma, A. Potthoff, L.-M. Berger, and C. Leyens, J. Therm. Spray Techn. **24**, 1143 (2015).
[21]J. W. Murray, G. A. Rance, F. Xu, and T. Hussain, J. Eur. Ceram. Soc. **38**, 1819 (2018).
[22]K. Shihommatsu, J. Takahashi, Y. Momiuchi, Y. Hoshi, H. Kato, and Y. Homma, ACS Omega **2**, 7831 (2017).
[23]H. Assadi, F. Gärtner, T. Stoltenhoff, and H. Kreye, Acta Mater. **51**, 4379 (2003).
[24]L. M. Malard, M. A. Pimenta, G. Dresselhaus, and M. S. Dresselhaus, Phys. Rep. **473**, 51 (2009).
[25]L. G. Cançado, A. Jorio, E. H. Martins Ferreira, F. Stavale, C. A. Achete, R. B. Capaz, M. V. O. Moutinho, A. Lombardo, T. S. Kulmala, and A. C. Ferrari, Nano Lett. **11**, 3190 (2011).
[26]M. S. Dresselhaus, A. Jorio, M. Hofmann, G. Dresselhaus, and R. Saito, Nano Lett. **10**, 751 (2010).
[27]E. Hsiao and S. H. Kim, Tribol. Lett. **35**, 141 (2009).
[28]S. Rengifo, C. Zhang, S. Harimkar, B. Boesl, and A. Agarwal, Technologies **5**, 4 (2017).
[29]W. Zhai, X. Shi, M. Wang, Z. Xu, J. Yao, S. Song, and Y. Wang, Wear **310**, 33 (2014).
[30]M. Tabandeh-Khorshid, E. Omrani, P. L. Menezes, and P. K. Rohatgi, Eng. Sci. Technol. Int. J. **19**, 463 (2016).
[31]H. J. Sharahi, G. Shekhawat, V. Dravid, S. Park, P. Egberts, and S. Kim, Nanoscale **9**, 2330 (2017).